

Calibration of a PEM Detector With Depth of Interaction Measurement

G.-C. Wang, *Student Member, IEEE*, J. S. Huber, *Member, IEEE*, W. W. Moses, *Senior Member, IEEE*, W.-S. Choong, *Member, IEEE*, and J. S. Maltz, *Member, IEEE*

Abstract—We present an *in situ* calibration technique for the LBNL positron emission mammography (PEM) detector module that is capable of measuring depth of interaction (DOI). The detector module consists of 64 LSO crystals coupled on one end to a single photomultiplier tube (PMT) and on the opposite end to a 64 pixel array of silicon photodiodes (PD). The PMT provides an accurate timing pulse, the PDs identify the crystal of interaction, the sum provides a total energy signal and the $\Gamma = \text{PD}/(\text{PD} + \text{PMT})$ ratio determines the depth of interaction. We calibrate using the ^{176}Lu natural background radiation of the LSO crystals. We determine the relative gain (K) of the PMT and PD by minimizing the asymmetry of the Γ distribution. We determine the depth dependence from the width of the Γ distribution with optimal K . The performance of calibrated detector modules is evaluated by averaging results from 12 modules. The energy resolution is a function of depth ranging from 24% FWHM at the PD end to 51% FWHM at the PMT end, and the DOI resolution ranges from 6 mm FWHM at the PD end to 11 mm FWHM at the PMT end.

Index Terms—Biomedical imaging, calibration, detectors, depth of interaction (DOI), positron emission tomography (PET).

I. INTRODUCTION

IN the design of positron emission tomography (PET) detectors, there is a tradeoff between sensitivity and spatial resolution. Increasing crystal length to achieve higher sensitivity leads to deterioration of spatial resolution due to the increased probability of detecting a gamma photon that has penetrated through more than one crystal. By measuring the depth of interaction within a crystal, it is theoretically possible to overcome the need to compromise either of these detector parameters. Depth of interaction can be measured using light sharing by placing a photon detector at both ends of a continuous scintillator crystal [1]–[3]. In the calibration of detectors that utilize light sharing, gain balancing between detectors is an essential step. The most obvious way of calibrating depth in a detector utilizing light sharing is to use a collimated gamma beam to excite the scintillator crystal at known depths. However, this is not feasible for a fully

assembled multicrystal detector, because the inner crystals are shielded from the excitation beam by their neighbors. One solution is to precalibrate each crystal before assembling the crystal array. However, *in situ* calibration is the only practical solution for ongoing calibration of the installed detectors. Such calibration is necessary to accommodate the effects of drift in photomultiplier tube gains, temperature sensitivity, and electronic aging.

The LBNL positron emission mammography (PEM) detector consists of 64 $3 \text{ mm} \times 3 \text{ mm} \times 30 \text{ mm}$ LSO crystals coupled to a single photomultiplier tube and an 8×8 silicon photodiode array [4]. The photomultiplier tube provides accurate timing. A custom PET readout IC (PETRIC) [5] amplifies the photodiode pulse signals and identifies the crystal of interaction by winner-take-all circuitry that chooses the crystal with the highest signal. The total energy is the sum of the photodiode and photomultiplier tube signals. Fig. 1 shows an assembled LBNL PEM detector.

For the LBNL PEM detector, the depth of interaction is determined by the ratio between the photodiode signal and the sum of the photodiode and photomultiplier tube signals [1]. Crystal dependent relative gains need to be determined to convert the photodiode and photomultiplier tube signals to the same energy scale. The challenge of this *in situ* calibration is to balance the gains between the photodiode and the photomultiplier tube signals, as well as obtain the transformation between the signal ratio and physical depth for each crystal. This paper describes a novel algorithm based on measuring the LSO background to determine the relative gain and depth dependence.

II. CALIBRATION ALGORITHM

A. Definitions

Fig. 1 depicts the LBNL PEM module and our coordinate conventions. The LBNL PEM module has 64 LSO crystals, which need to be calibrated individually. For a given i th crystal, $\text{PMT}'_i(x)$ and $\text{PD}'_i(x)$ denote the uncorrected photopeak positions of the photomultiplier tube and the photodiode array signals when excited at a depth of x , respectively. The relative gain K_i is defined as

$$K_i = \frac{\text{PMT}'_i(x = 30 \text{ mm})}{\text{PD}'_i(x = 0 \text{ mm})}. \quad (1)$$

The gain-corrected photodiode bin is defined as

$$\text{PD}_i(x) = K_i \times \text{PD}'_i(x). \quad (2)$$

Manuscript received November 15, 2003; revised February 17, 2004. This work was supported in part by the Director, Office of Science, Office of Biological and Environmental Research, Medical Science Division, U.S. Department of Energy under Contract DE-AC03-76SF00098, and in part by National Institutes of Health Grant RO1-CA67911. Reference to a company or product name does not imply approval or recommendation by the University of California or the U.S. Department of Energy to the exclusion of others that may be suitable.

The authors are with the Lawrence Berkeley National Laboratory, Berkeley, CA 94720 USA (e-mail: gcwang@lbl.gov).

Digital Object Identifier 10.1109/TNS.2004.829785

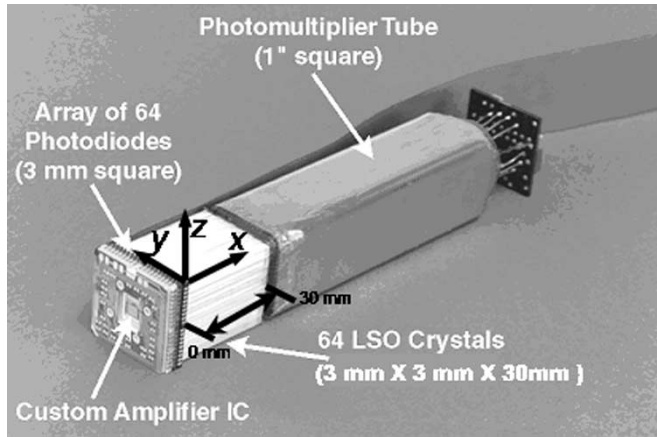


Fig. 1. Picture of the LBNL PEM module. The LSO crystals are sandwiched between a PMT and photodiode array. The x here denotes the depth of interaction axis, which is defined to be zero at the photodiode end.

The depth estimator Γ_i is defined as

$$\Gamma_i = \frac{PD_i(x)}{PMT_i(x) + PD_i(x)} = \frac{K_i \times PD'_i(x)}{PMT_i(x) + K_i \times PD'_i(x)} \quad (3)$$

which is approximately linear in x for all crystals [6].

When histogramming the signals from the PD and PMT individually, the pulse-height spectra of a typical crystal are shown in Fig. 2(a) and (b). Although peaks are observed in these distributions, the typical features such as a well-defined photopeak and Compton shoulder are not seen since the light is shared between two detectors. Because the scintillation photons are shared in a depth-dependent ratio between the PD and PMT, exciting the crystal at different depths results in different PD and PMT pulse-height spectra [4]. This depth dependence results in smeared pulse-height spectra that are the sum of pulse-height spectra at all interaction depths weighted by the probability of an interaction occurring at the given depth. However, summing the calibrated PD and PMT signals restores the total energy, producing an improved pulse-height spectrum of the sum (PD + PMT) as shown in Fig. 2(c). (It is worth noting that an improper relative gain K_i eliminates the photopeak. Therefore, a well-defined photopeak can be used to confirm that the relative gain K_i is chosen properly.)

B. Initial Setup

1) *Photodiode Array Setup*: Each PETRIC chip processes signals from 64 photodiode pixels. The photocurrent from the photodiode array is collected and processed by the PETRIC to determine the address and signal amplitude of the interacting crystal. A fully functional PETRIC requires several internal registers and bias voltages to be configured correctly. Two bias voltages (controlled by digital potentiometers) adjust the rise and fall time of all the shapers in the PETRIC. In practice, they are manually adjusted to give a $1.2 \mu\text{s}$ peaking time which maximizes the signal-to-noise ratio (SNR) of the pulse signal [5]. This peaking time is the dominant contribution of the dead time of the module. Preamplifier gains of the PETRIC are set to their

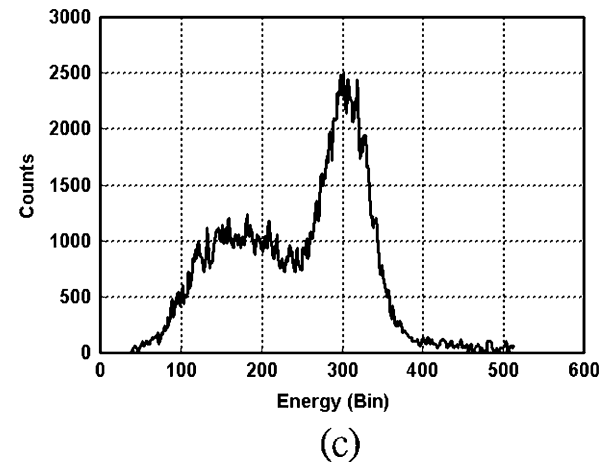
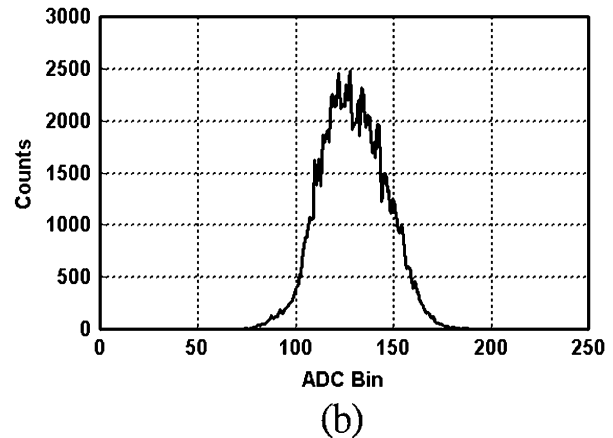
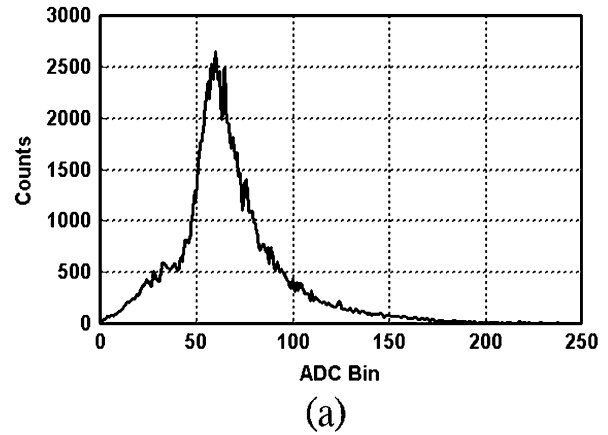


Fig. 2. Pulse-height spectrum of a typical crystal from (a) PMT signal, (b) PD signal, and (c) the sum of the calibrated PD and PMT signals. The same event sample is used for all plots.

maximum value for all channels. A reset current that compensates for photodiode leakage current is required for each channel to prevent the charge-sensitive-amplifier from saturating. For each channel, an electronic test pulse is injected and the reset current is increased until the output amplitude of the amplifier reaches a plateau. This procedure finds the reset current that minimizes the amplifier electronic noise. Channel pedestals (quiescent level of the amplifier output) are also measured and recorded.

2) *Photomultiplier Tube Setup*: A dedicated ASIC from CPS Innovations (Knoxville, TN) [7] processes the PMT pulse.

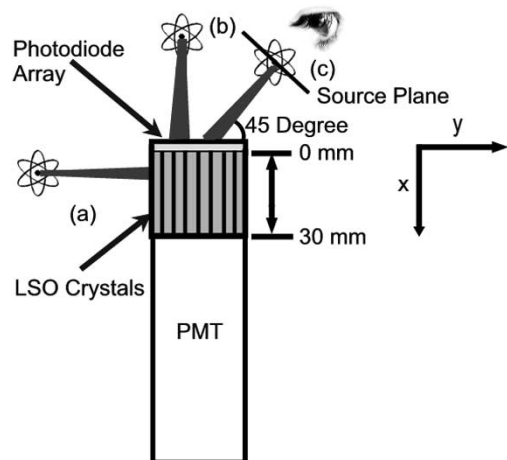


Fig. 3. Experimental setups used to validate and perform the calibration. An electronically collimated beam of 511 keV gamma rays is incident (a) normal to the side, (b) normal to the face, and (c) at a 45° angle to the face of the LSO crystal array.

“Singles” events are used to set up the PMT ASIC. A ^{68}Ge point source is positioned as shown in Fig. 3(b) to excite with 511 keV gammas. The preamplifier gain of the PMT ASIC is adjusted until the peak of the pulse-height spectrum is close to one-third of the maximum ADC bin. This allows us to make full use of the ADC dynamic range. The constant-fraction-discriminator (CFD) threshold is set low enough so that the Compton shoulder in the pulse-height spectrum is observed, but high enough to avoid an excessive count rate.

3) *Readout Electronics Setup*: The electronic system described in [8] is used to read out the detectors. The system consists of 14 analog subsection boards, 4 detector head interface boards, and a coincidence controller. For calibration, the analog subsections are set to pass the interacting crystal address, photodiode and photomultiplier tube signal amplitudes to the coincidence controller. The coincidence controller is set to pass-through mode, in which it simply packs the data from the analog subsections into “singles” event words and sends these words to the host computer.

C. Relative Gain

LSO is naturally radioactive due to the presence of ^{176}Lu [9]. The decay process consists of a beta decay followed by a gamma cascade. It is reasonable to assume that the ^{176}Lu is homogeneously distributed inside the LSO crystal. Based on this assumption, the radioactivity along the depth direction within the LSO crystal should be distributed symmetrically owing to the symmetric geometry of the crystal (see Fig. 4).

“Singles” events are collected from the LSO background without using an external source. The intensity of the natural background radiation is 300 decays/s/cm³. In our case, a 100 second acquisition time provides roughly 8000 events per crystal, which is enough for relative gain calibration. Since the depth estimator (Γ_i) is approximately a linear function of position x , the histogram of the Γ_i distribution from “singles” events of LSO background (with the correct relative gain K_i) should also be symmetric.

Skewness (defined as the third central moment divided by the third power of the standard deviation of a distribution) describes

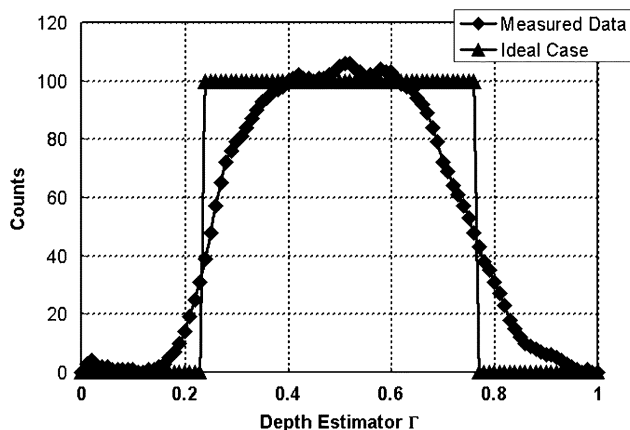


Fig. 4. Ideally, the background radioactivity exhibits an uniform distribution along the depth of the crystal. In practice, the measured data (after calibration) are symmetric about the center of the crystal but fall off near the edges owing to the noise of the amplifiers and escaping gammas at the edges.

the degree of asymmetry of a distribution, and a symmetric distribution exhibits zero skewness. With the optimal relative gain K_i , the skewness of the Γ_i distribution falls to zero. This numerical one-dimensional zero crossing problem is solved by Newton’s method. Fig. 5 shows an example of determining the optimal K_i . A too small K_i leads to a left-skewed Γ_i distribution, and a too large K_i leads to the opposite. Only the proper K_i corresponds to a symmetric Γ_i distribution.

D. Depth Dependence

After determining the optimal relative gain K_i , a linear transformation is needed to convert a given Γ_i to the corresponding physical depth for the i th crystal. To attain this linear relation, we process the same raw set of LSO background data with the optimal K_i and look at the Γ_i distribution of background events. The physical edges of the crystal in the depth direction are highly correlated to the rising and falling edges of the background Γ_i distribution (see Fig. 6). The rising and falling edges are identified empirically as the positions where the height of Γ_i is one-third of the maximum count of the background Γ_i distribution.

The goal of the LBNL PEM module is to resolve eight depth bins [8]. In other words, the goal is to divide the crystal into eight segments in the depth direction. This segmentation is equivalent to dividing the region between the rising and falling edge of the background Γ_i distribution into eight segments of equal width. A given Γ_i that is within the range of a segment is assigned to the corresponding depth bin. Mathematically, the depth bin for i th crystal is determined as follows:

$$\text{bin}_i = \text{Floor} \left(\frac{8 \times (\Gamma_i - (\Gamma_R)_i)}{(\Gamma_F)_i - (\Gamma_R)_i} \right) \quad (4)$$

where $(\Gamma_R)_i$ and $(\Gamma_F)_i$ denote the rising and falling edges (both at 1/3 maximum) of the background Γ_i distribution, respectively. A typical 2 GHz PC can both collect the necessary data and compute the K_i and depth factors for 64 crystals within 10 min.

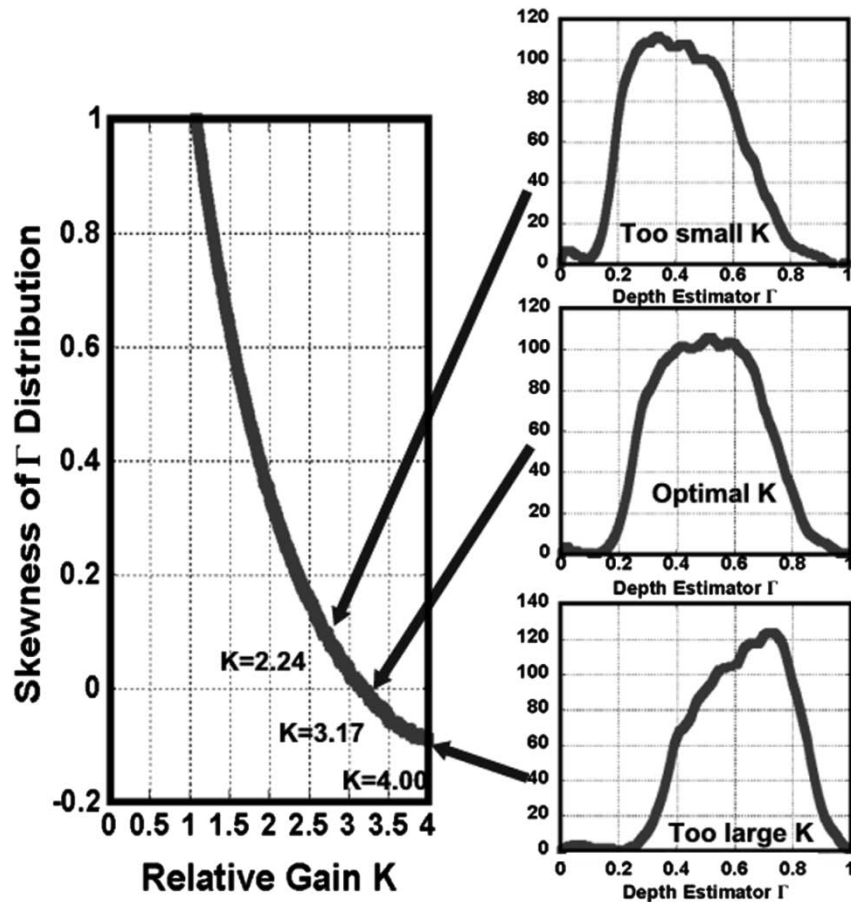


Fig. 5. Skewness as a function of relative gain K for a typical crystal. The corresponding Γ distributions are shown for specific K values. The zero crossing of this crystal is at approximately $K = 3.17$.

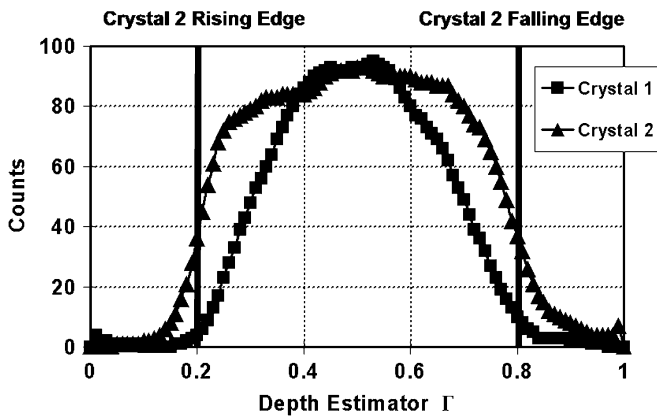


Fig. 6. Distributions of the depth estimator Γ for two crystals using LSO background "singles." Crystals with larger depth dependence have wider Γ distributions. The bars denote the rising and falling edges of crystal 2. A value of $\Gamma = 0.3$ converts to the 0th depth bin for crystal 1 but 1st depth bin for crystal 2.

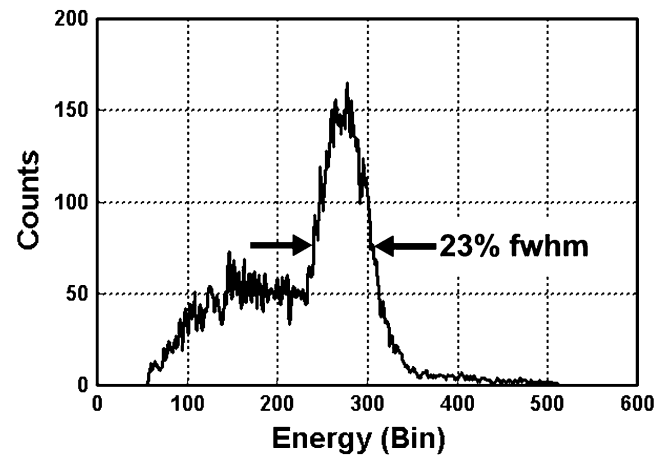


Fig. 7. Pulse-height spectrum of a typical crystal at 0th depth bin (from 0 to 3.75 mm from the PD end). An energy resolution of 23% FWHM is measured.

III. RESULTS AND VALIDATION

A. Energy Resolution

"Singles" events from 692 crystals are taken with front excitation of a ^{68}Ge point source as illustrated in Fig. 3(b). Data are collected with the LBNL PEM electronic system and processed offline with the calibration parameters obtained from the algorithm described in Section II.C. Histogramming the sum of

the PMT and gain-corrected PD signals produces pulse-height spectra. Fig. 7 shows the pulse-height spectrum of a typical crystal with interactions that occur in the 0th depth bin (depth ranges from 0 to 3.75 mm from the PD end); the energy resolution is 23% full width at half maximum (FWHM).

The energy resolution is a function of depth. Fig. 8 shows the distribution of energy resolutions of 692 crystals for the 0th and 4th depth bins. The energy resolution degrades at higher depth bins because the SNR of the photodiode is worse for events

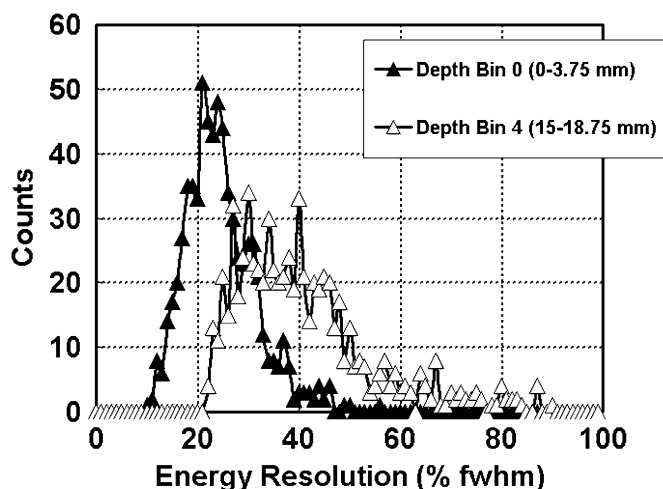


Fig. 8. Histograms of energy resolution (for two depths bins) of 692 crystals in 12 detector modules. The average energy resolution is 24% FWHM for the 0th depth bin and 41% FWHM for the 4th depth bin.

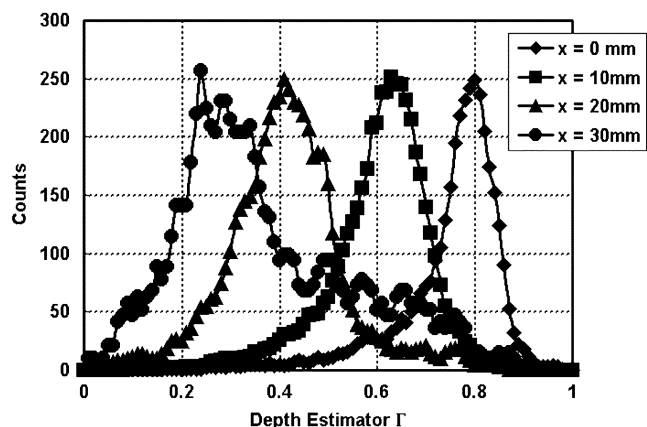


Fig. 9. Γ distributions at four excitation depths for a single crystal. The FWHMs of the Γ distribution are 0.11, 0.16, 0.19, and 0.20 bin respectively, which correspond to 5.5, 8.0, 9.5, and 10.0 mm FWHM DOI resolution.

that occur near the PMT end of the crystal [6] (the photodiode noise is a constant but the signal depends on depth, so the SNR is a function of depth). The average energy resolution ranges from 24% FWHM at the photodiode end (0th depth bin) to 51% FWHM at the photomultiplier tube end (7th depth bin).

B. DOI Resolution

We validate our calibration technique by exciting the modules from the side as illustrated in Fig. 3(a). An electronically collimated beam of 511 keV gamma rays excites a 3 mm FWHM portion of the crystals. The collimated beam is scanned through the crystals at fixed x positions using an XYZ stage in 5 mm increments from 0 to 30 mm. Data from 62 crystals are taken to verify the excitation depth versus Γ relation. The 511 keV gamma beam is attenuated through the LSO crystals. Consequently, only the first three layers of the edge crystals record sufficient events to validate their calibration. Fig. 9 shows the Γ_i distributions for a typical crystal with the module excited at four different depths ($x = 0, 10, 20,$ and 30 mm respectively). The dependence of the centroid of the Γ_i distribution on the ex-

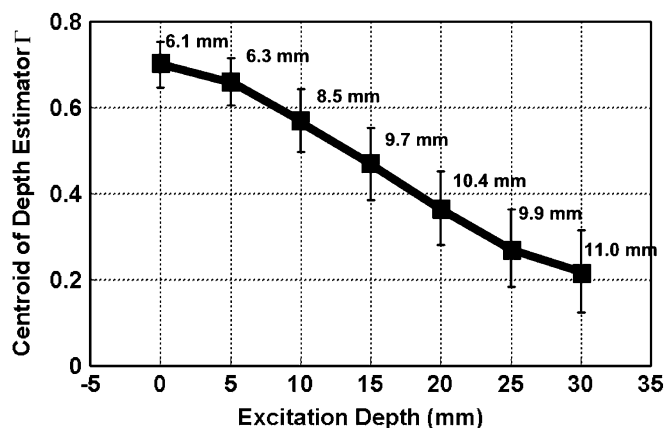


Fig. 10. Average centroids of Γ are plotted and labeled with calculated DOI resolutions for seven excitation depths. Measurements are averaged over 62 crystals. Selected events have $250 < E < 750$ keV energy deposit. A 3 mm FWHM portion of the LSO crystal is excited.

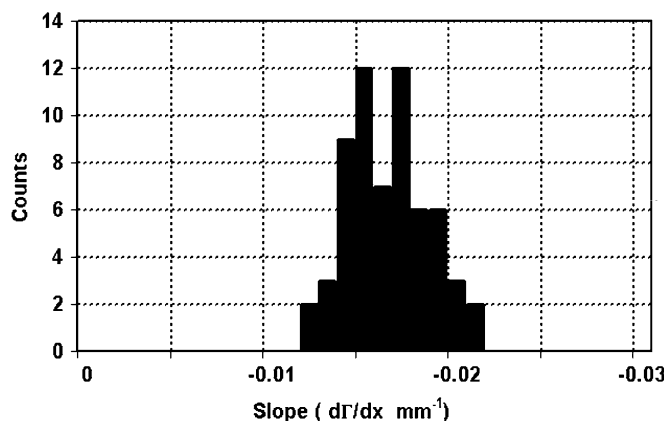
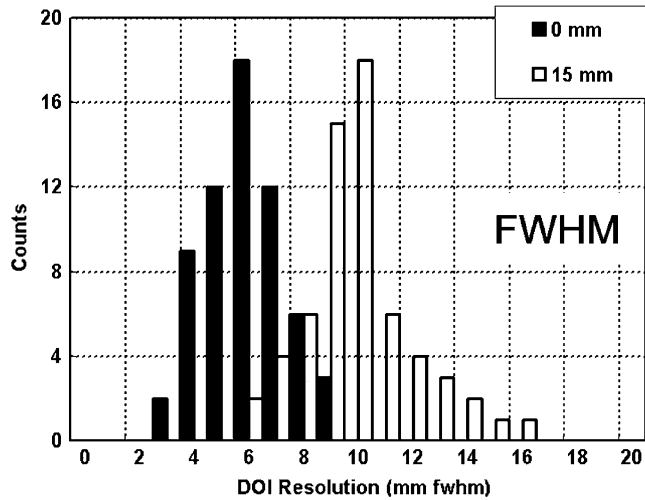


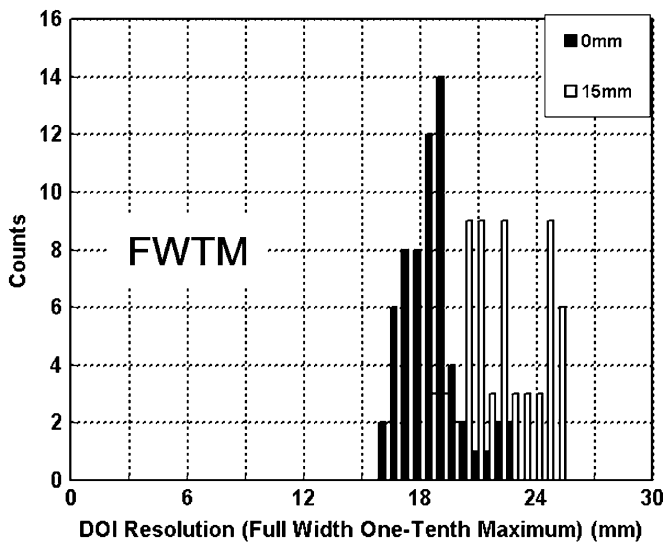
Fig. 11. Distribution of fitted slopes of Γ_i versus excitation depth x from 62 crystals. The slopes range from -0.013 to -0.021 mm^{-1} .

citation depth x is clearly shown. Fig. 10 shows the relationship between the excitation depth x and the average centroid of the Γ_i distribution for 62 crystals. For each individual crystal, the centroid of the Γ_i distribution depends linearly on the excitation depth x (for each of the 62 crystals, the linear fitting exhibits a correlation coefficient greater than 0.98). The crystal to crystal variation in this fitted slope is also important. Fig. 11 shows the distribution of the slopes. The slopes range from -0.013 to -0.021 mm^{-1} . Therefore, it is necessary to perform depth dependence calibration for each crystal.

The DOI resolution is defined as the FWHM of the Γ_i distribution divided by the slope of the least square fit of Γ_i versus excitation depth x [6]. Because the width of the Γ_i distribution depends on depth, the DOI resolution is a function of depth. The crystal shown in Fig. 9 has a DOI resolution of 5.5 to 9.5 mm FWHM. Fig. 12 shows the distribution of DOI resolutions of 62 crystals when excited at the depths of 0 and 15 mm. The average DOI resolution is 6.1 mm FWHM at the PD end and degrades to 11 mm FWHM at the PMT end (see Fig. 10). This degradation is also due to the decreased SNR as described for energy resolution in the previous section. The DOI resolution has improved in comparison to a previous prototype module, which had 6 to



(a)



(b)

Fig. 12. (a) Histograms of FWHM DOI resolution (for two excitation depths) for 62 crystals. The average DOI resolution is 6.1 mm FWHM when excited at the depth of 0 mm and 9.7 mm FWHM when excited at the depth of 15 mm. (b) Histograms of DOI resolution (for two excitation depths) using full width at one-tenth maximum for 62 crystals.

15 mm DOI resolution [4]. This improvement may be attributed to the lower electronic noise of the PETRIC.

A comparison between the calibration constants obtained with the side excitation and the background radiation methods is shown in Fig. 13. The proximity of the data to the 45° ($x = y$) line indicates that the background radiation method is in agreement with the side excitation method.

C. Module Performance

To produce images that illustrate the performance of the calibrated DOI detector, data are taken with the setup as shown in Fig. 3(c). An electronically collimated beam of 511 keV gamma rays is incident at a 45° angle onto the face of the LSO crystal array. With the correct calibration, the measured position of the interaction should lie on a 45° beam line in the x - y plane. We process the data using the calibration factors derived from our algorithms, and determine the depth bin_{*i*} using (4). The events are assigned to three-dimensional positions within the

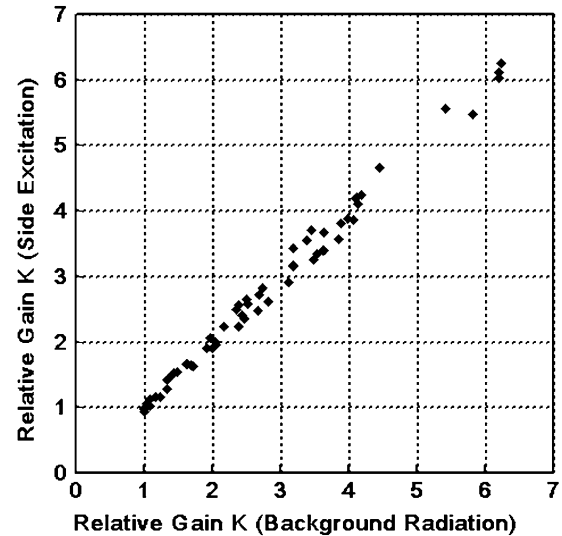


Fig. 13. Scatter plot of optimal relative gain K obtained from the side excitation and the background radiation methods. It is clear that the data lie closely to the 45° ($x = y$) line.

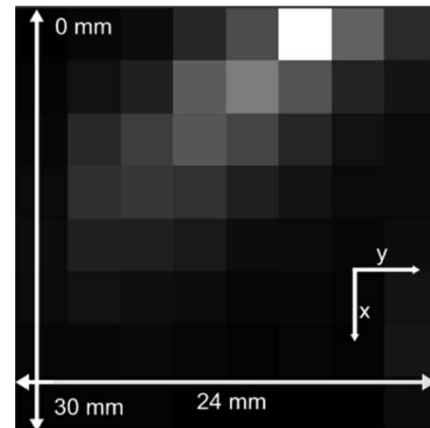


Fig. 14. Image of a collimated beam of gamma rays incident at 45° onto the face of one detector module. The image shows the projection of the LSO array onto x - y plane. Selected events have $250 < E < 750$ keV energy deposit.

module, and the number of events at each position is stored in an $8 \times 8 \times 8$ array (8×8 crystals, and 8 depth bins for each crystal). Only the events within a 250–750 keV energy window are selected. Fig. 14 shows the x - y projection image of this array. The 45° angle of the beam is clearly visible and the exponential attenuation of the beam with depth is also evident. The results validate the correctness of the assigned depth bins.

Using the data that is displayed in Fig. 14, we can image the ^{68}Ge point source by backprojecting the array to the source plane as indicated in Fig. 3(c). Fig. 15(a) shows the image by backprojecting the whole $8 \times 8 \times 8$ array when DOI information is used. Fig. 15(b) shows the image reconstructed without DOI information by assigning all interactions to the 0th depth bin, i.e., the front face of the LSO array. The reduced blurring due to the DOI capability is clearly visible.

IV. DISCUSSION

The calibration of a volumetric radiation detector poses unique challenges. Ideally, one would calibrate such a detector

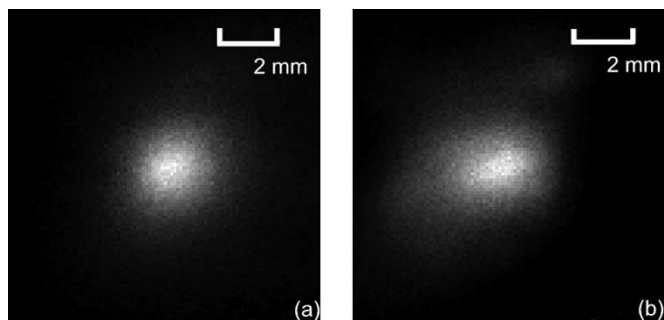


Fig. 15. Images of the ^{68}Ge point source. (a) The backprojected image with DOI information. The symmetry of the point source is preserved because of the DOI capability. (b) The backprojected image without DOI information. The image suffers from penetration artifacts. Both images are generated from the same set of data. The field of view is 1 cm square.

by exciting a single point inside the crystal array. However, the feasible option is to employ a collimated gamma beam to produce a line of excitation. There are two major problems with the collimated beam line: 1) the distribution of excitation is far from a perfect line because of scattering and attenuation and 2) the geometry of the detector and camera usually limits the directions and positions of this beam. However, not all detector designs suffer this difficulty. For example, phoswich detectors that use layer dependent decay time to encode depth do not exhibit this problem.

Many prototype DOI module designs have been calibrated using side excitation [10], [11]. For these studies, depth calibration is straightforward since only a few crystals or channels are present. However, once the prototype is scaled up to a full-sized module and placed in a camera, an *in situ* calibration is required. The known activity distribution of the internal radioactive source (e.g., the ^{176}Lu in the LSO crystal) can be used to adjust and optimize the calibration parameters in volumetric detectors, which is especially helpful in designs that use the analog ratio of signals to measure depth.

When developing new detectors, one could even add radioisotopes to nonradioactive scintillators to employ this calibration scheme. If so, it may be preferable to add radioisotopes that produce radiations that do not overlap with the energy window of the radiotracer being imaged.

V. CONCLUSION

We have developed and validated an *in situ* calibration algorithm for the LBNL PEM camera. This algorithm has three advantages: 1) no external source is needed for relative gain cal-

ibration; 2) data for calibration can be taken simultaneously for all crystals because the ^{176}Lu background radioactivity resides in every LSO crystal; and 3) little computation power is needed to process the data.

The performance of the calibrated modules has been evaluated. The results show that the average energy resolution ranges from 24% FWHM at the PD end to 51% FWHM at the PMT end. The DOI resolution is also a function of depth and ranges from 6 mm FWHM at the PD end to 11 mm FWHM at the PMT end. Our calibration method can be applied to most PET detector designs that use an analog ratio of signals to measure depth. The algorithm is independent of the length of the crystal as long as the signals can be measured with enough SNR.

ACKNOWLEDGMENT

The authors thank CPS Innovations, Knoxville, TN, for providing electronics and technical assistance.

REFERENCES

- [1] W. W. Moses and S. E. Derenzo, "Design studies for a PET detector module using a PIN photodiode to measure depth of interaction," *IEEE Trans. Nucl. Sci.*, vol. 41, pp. 1441–1445, 1994.
- [2] Y. P. Shao and S. R. Cherry, "A study of depth of interaction measurement using bent optical fibers," *IEEE Trans. Nucl. Sci.*, vol. 46, pp. 618–623, 1999.
- [3] Y. Shao *et al.*, "Design studies of a high resolution PET detector using APD arrays," *IEEE Trans. Nucl. Sci.*, vol. 47, pp. 1051–1057, 2000.
- [4] J. S. Huber *et al.*, "A LSO scintillator array for a PET detector module with depth of interaction measurement," *IEEE Trans. Nucl. Sci.*, vol. 48, pp. 684–688, 2001.
- [5] M. Pedrali-Noy, G. J. Gruber, B. Krieger, E. Mandelli, G. Meddeler, V. Rosso, and W. W. Moses, "PETRIC—A positron emission tomography readout IC," *IEEE Trans. Nucl. Sci.*, vol. 48, pp. 479–484, 2001.
- [6] W. W. Moses, S. E. Derenzo, and C. L. Melcher, "A room temperature LSO/PIN photodiode PET detector module that measures depth of interaction," *IEEE Trans. Nucl. Sci.*, vol. 42, pp. 1085–1089, 1995.
- [7] D. M. Binkley *et al.*, "A custom CMOS integrated circuit for PET tomograph front-end applications," in *Proc. IEEE 1993 Nuclear Science Symp./Medical Imaging Conf.*, L. Klaisner *et al.*, Ed., San Francisco, CA, 1993, pp. 867–871.
- [8] W. W. Moses *et al.*, "The electronics system for the LBNL positron emission mammography (PEM) camera," *IEEE Trans. Nucl. Sci.*, vol. 48, pp. 632–636, 2001.
- [9] C. L. Melcher and J. S. Schweitzer, "Cerium-doped lutetium oxyorthosilicate: A fast, efficient new scintillator," *IEEE Trans. Nucl. Sci.*, vol. 39, pp. 502–505, 1992.
- [10] Y. Shao *et al.*, "Dual APD array readout of LSO crystals: Optimization of crystal surface treatment," *IEEE Trans. Nucl. Sci.*, vol. 49, pp. 649–654, 2000.
- [11] E. Gramsch, R. Avila, and P. Bui, "Measurement of the depth of interaction of an LSO scintillator using a planar process APD," *IEEE Trans. Nucl. Sci.*, vol. 50, pp. 307–312, 2003.